

---

# The Circulation and Hydrography of Conception Bay, Newfoundland

Brad deYoung  
Department of Physics  
Memorial University of Newfoundland  
St John's, Newfoundland, Canada A1B 3X7

and

Brian Sanderson  
Bureau of Meteorology Research Centre  
GPO Box 1289K, Melbourne  
Victoria 3001, Australia

[Original manuscript received 28 August, 1992; in revised form 6 September 1994]

---

**ABSTRACT** *The hydrography and circulation of Conception Bay (Newfoundland) are described based on hydrographic, current-meter and drifter data collected over four years (1988–1991). The seasonal cycles of temperature ( $-1.6$  to  $13-17^{\circ}\text{C}$ ) and salinity ( $31-32.5$ ) in the bay closely follow those on the adjacent shelf. Exchange of bottom water was observed in April 1989. Deepwater exchange was observed from late fall to early winter of 1989–90. Tidal currents are weak,  $1-2\text{ cm s}^{-1}$  for the  $M_2$  and  $K_1$  constituents. Observed Eulerian mean currents ( $<3\text{ cm s}^{-1}$ ) are smaller than the standard deviation ( $1-11\text{ cm s}^{-1}$ ); however, there is a persistent outflowing current of  $10$  to  $20\text{ cm s}^{-1}$  within  $2\text{ km}$  of the shoreline on the eastern side of the outer bay. The Lagrangian correlation length scale is from  $4$  to  $10\text{ km}$ , in agreement with the weak coherence squared ( $\leq 0.4$ ) found between the fixed current-meter sites separated by greater than  $4-5\text{ km}$ . The variable currents (up to  $20\text{ cm s}^{-1}$ ) tend to be cyclonic. Cyclonic eddies were observed near the mouth on the eastern side of the bay, adjacent to the outflow. A simplified fractal dispersion model gives residence times of  $42\text{ d}$  similar to those obtained from a scaling analysis ( $30-40\text{ d}$ ) and a diagnostic numerical model ( $30\text{ d}$ ).*

**RÉSUMÉ** *On décrit l'hydrographie et la circulation dans la baie Conception (T.-N.) en se basant sur des données hydrographiques, de courantomètres et de dériveurs enregistrées durant quatre ans (de 1988 à 1991). Les cycles saisonniers de température ( $-1,6$  à  $13,7^{\circ}\text{C}$ ) et de salinité ( $31$  à  $32,5$ ) de la baie sont très près de ceux de la plate-forme voisine. On a observé un échange d'eau de fond en avril 1989. Un échange en eau profonde a eu lieu de la fin d'automne au début de l'hiver 1989/90. Les courants de marée sont faibles,  $1$  à  $2\text{ cm s}^{-1}$  pour les éléments  $M_2$  et  $K_1$ . Les courants eulériens moyens observés ( $< 3\text{ cm s}^{-1}$ ) sont plus petits que l'écart type ( $1$  à  $11\text{ cm s}^{-1}$ ); toutefois, il y a un courant sortant persistant*

*de 10 à 20 cm s<sup>-1</sup> à moins de 2 km du rivage sur le côté est de l'avant-baie. La corrélation lagrangienne de l'échelle de longueur est de 4 à 10 km, s'accordant avec la faible cohérence mise au carré ( $\leq 0,4$ ) trouvée entre les sites des courantomètres fixes séparés par plus de 4 à 5 km. Les courants variables (jusqu'à 20 cm s<sup>-1</sup>) tendent à être cycloniques. On a observé des tourbillons cycloniques près de l'embouchure est de la baie, voisins du flux sortant. Un modèle de dispersion fractale simplifié montre des temps de séjour de 42 jours, semblables à ceux obtenus d'une analyse d'échelle (30 à 40 jours) et un modèle numérique de diagnostique (30 jours).*

---

## 1 Introduction

The circulation and forced response of large coastal embayments are interesting for many reasons. Because of the coastal boundary condition, convergent and divergent flow fields are set up, forced by either the wind or the tides. Coastal trapped waves are present at low frequencies as continental shelf waves, and at higher frequencies as Kelvin waves (Csanady, 1982). Other processes such as internal tides, bottom boundary layers, and deep-water exchange can also be studied in this coastal environment. In addition, coastal bays are biologically active and ecologically diverse, and because of their relative ease of access, provide good areas in which to study complex systems that are usually undersampled. In bays the velocity and density fields can have large vertical and horizontal gradients and respond strongly to wind forcing, making bays dynamic regions in which to explore the link between biological and physical variables. In this paper we shall present results of a physical oceanographic study of Conception Bay, Newfoundland, that was carried out as part of the Cold Ocean Productivity Experiment (COPE), a joint biological-physical project to determine bacterial and primary production in cold high-latitude waters (Pomeroy et al., 1991).

An earlier physical study, conducted in the summer of 1985, did provide some preliminary information on the physical oceanographic features of the bay (Aggett et al., 1987). Three current-meter moorings were deployed indicating (i) weak tides and (ii) a relatively weak mean flow. The motivation of the present study was to describe and model the mean circulation in the bay, the wind-forced response and the development of the thermocline structure, in particular during the spring period when primary production is at its greatest (Pomeroy et al., 1991). This work is part of several related studies on the bay. A diagnostic calculation was developed for the bay (deYoung et al., 1993a) using density data from several different periods. The resulting velocity fields show that the bay has no single dominant circulation pattern, although there are persistent features. The wind-forced response of the bay was investigated using a reduced-gravity model (deYoung et al., 1993b), which showed the influence of neighbouring Trinity Bay on the internal response of Conception Bay. A local and non-local wind-forced response was detected in the bay, with the non-local response dominating on the western side of the bay near the mouth. The velocity field from the diagnostic model was used (deYoung et al.,

1994) to estimate the residence time for capelin larvae in the bay. The advection-diffusion model of the larvae suggested a residence time of roughly 30 days for surface waters near the head of the bay.

In this paper we present the results of four years of oceanographic work in Conception Bay from 1988 to 1991. We provide a description of this physical system that will be useful as an example of a coastal embayment and also as a framework in which to understand some of the earlier and ongoing biological studies. The outline of the paper is as follows. In Section 2 we describe the study area, and provide a description of the field work carried out and of the physical data obtained. In Section 3, the hydrography of the bay is described and some analysis is presented of the seasonal variability both in the bay and just outside. Section 4 contains a description of the circulation based upon the Eulerian measurements. Section 5 presents the Lagrangian data. A discussion of the results and a scale analysis for the bay is presented in Section 5 followed in Section 6 by a brief summary.

### 2 Study area and methods

Conception Bay is a long (70–100 km) and narrow ( $\sim 20$ –30 km at the mouth) bay on the east coast of the island of Newfoundland (see Fig. 1). The bay is wide compared with the internal Rossby radius ( $\sim 1$ –10 km) but narrow relative to the external Rossby radius ( $\sim 500$  km). The maximum depth in the bay is about 300 m in the central basin. At the mouth there is a sill at about 150-m depth that closes off isobaths in the bay and restricts deep water access. Figure 1 shows that the bottom slope is steep near the shore; indeed, cliffs up to 250 m surround most of the Bay. There are three small islands (Bell, Little Bell and Kellys islands) of varying sizes located on the southeast side of the bay, a shallow region with depths  $\leq 60$  m (also see Fig. 2).

Pack ice often covers the bay from mid-March to late April, though little ice is formed locally in the bay (Cote, 1989). The local ice concentration in late winter is primarily influenced by ice on the shelf offshore and the presence of onshore winds in the late winter period. Local freshwater runoff is relatively unimportant compared to the influence of ice-melt upstream of the bay, which dominates the surface salinity variability. It is this non-local ice-melt which causes a late-summer minimum in the surface salinity (Mertz et al., 1993).

Conception Bay opens up onto the Avalon Channel, a pathway for the inshore branch of the Labrador Current (Petrie and Anderson, 1983). Flow in this channel is southward with a mean near-surface speed of roughly  $20 \text{ cm s}^{-1}$ . Horizontal coherence scales for the low-frequency motion in the channel are low, probably because of instability in the flow. Anderson (1986) showed that the vertical coherence was strong, except near the coast, but horizontal coherences were insignificant at spatial scales beyond 20 km.

Field work was conducted in Conception Bay from 1988 to 1991. CTD casts were made at about 30–40 stations in the bay (Fig. 2) on 14 cruises conducted

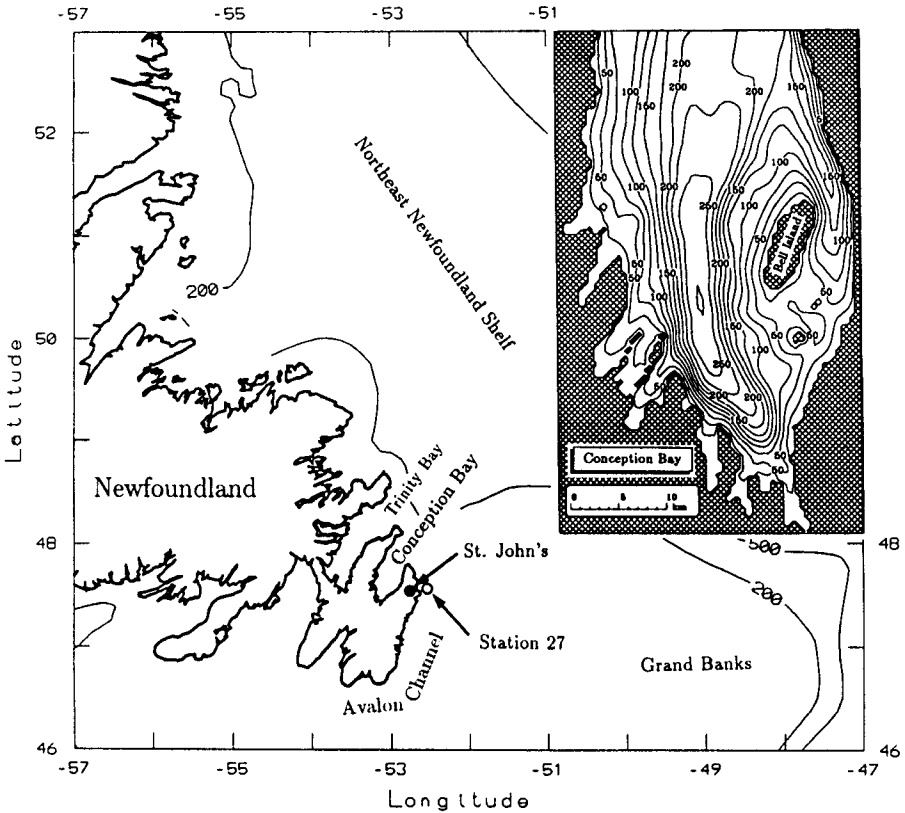


Fig. 1 The bottom topography of the Newfoundland shelf showing the location of Conception Bay. Depth contours are in metres. The detailed topography of the bay is shown in the inset.

over the four-year period. Not all stations were sampled during each cruise but all the stations were occupied at least twice during each year. On some of the cruises, stations were occupied in the Avalon Channel. Two CTDs were used: a Neil Brown MkIIIB and a Seabird SBE25. Calibrations and regular field checks were performed on both instruments giving an accuracy of better than  $0.01^{\circ}\text{C}$ , 0.01 for salinity and 0.01 for  $\sigma_t$ . In addition to the standard sensors, the SBE25 also carried a LiCor light sensor, a Seatech fluorometer and transmissometer. Observations from these instruments were quality checked and averaged to produce smoothed data at 1-m vertical resolution.

Current-meter moorings were deployed in three of the four years. Locations of the moorings deployed in 1989 and 1990 are shown in Fig. 2b. The longest time series comes from the 1989 deployment when  $\sim 160$  days of data were obtained from April to October. The two mooring deployments were directed towards different oceanographic problems. The 1989 array focussed on the mouth of the bay with

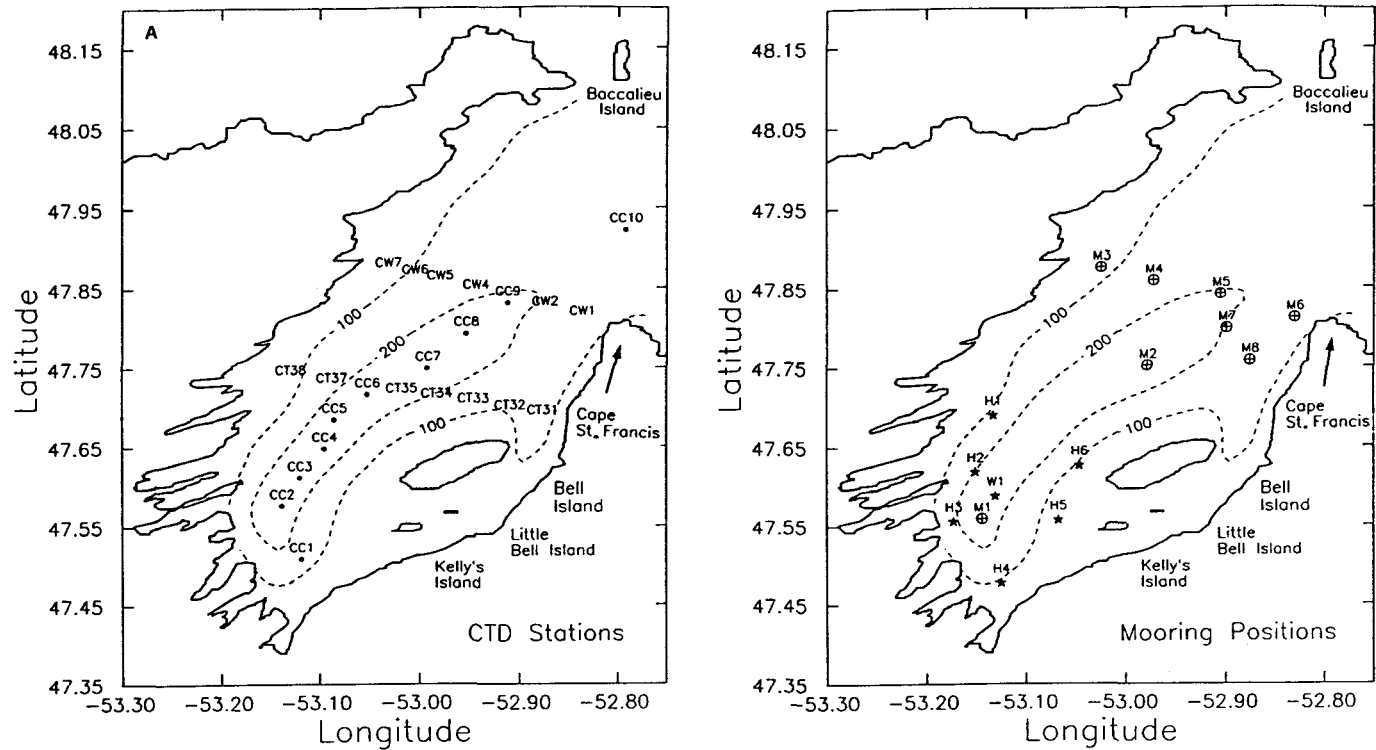


Fig. 2 (a) Locations of the CTD stations occupied during the project. Selected stations discussed in detail are marked. (b) Locations of the current-meter moorings in 1989 and 1990. The moorings deployed in 1989 (M1–M8) are marked with a circle with a cross inside. The moorings deployed in 1990 (H1–H6) and in the winter of 1989/90 are marked with a solid star. Dashed lines show the 100- and 200-m isobaths.

## 140 / Brad de Young and Brian Sanderson

TABLE 1. Times and types of drifter experiments conducted in Conception Bay 1987–1991.

Start Date	Finish Date	Number	Drifter Type	Release Position
24-9-87	26-9-87	5	Argos	4 km W Kellys
26-7-88	28-7-88	30	Radar-1	3 km W Kellys
1-8-88	5-8-88	29	Radar-1	3 km W Kellys
8-8-88	10-8-88	18	Radar-1	6–7 km W Kellys
4-9-88	4-9-88	15	Radar-1	between Kellys and Bell
5-9-88	5-9-88	15	Radar-1	between Kellys and Bell
4-4-89	6-4-89	9	Radar-2	6 km SW Kellys
19-4-89	24-4-89	12	Radar-2	6 km SW Kellys
31-5-89	31-5-89	12	Radar-1	8 km W Kellys
1-6-89	1-6-89	12	Radar-1	6 km W Kellys
2-6-89	2-6-89	8	Radar-1	6 km SW Kellys
3-7-89	13-7-89	11	Radar-2	throughout bay
31-10-89	4-11-89	1	Loran-C	outer bay (25 m)
1-11-89	4-11-89	8	Radar-2	5–8 km SW Kellys
3-7-91	13-7-91	6	Loran-C	outer bay (10 m)

the intention of defining the circulation across the mouth and providing boundary conditions for a numerical model. The 1990 program, with moorings deployed around the head of the bay, focussed on understanding the wind-forced response in the Kelvin waveguide around the bay. All the current meters measured temperature and conductivity, and some carried pressure sensors. In 1989, Aanderaa RCM4s and RCM7s were used with paddle wheel rotors. The RCM7s were deployed in the near-surface layer, nominally at 20-m depth, and the RCM5s near the bottom at roughly 100–150 m depth. In 1989, three thermistor chains with vertical resolution of 5–10 m were recovered from moorings M3, M4 and M5. The thermistor chain at M1 was lost in 1989. In 1990 a similar mooring structure was used except that InterOcean S4 current meters were deployed in the near-surface layer. All the bottom current meters were Aanderaa RCM5s or RCM7s, at nominal depths of 100 m. Three thermistor chains produced useful data in 1990, from mooring sites H2, H4 and H5. One mooring was deployed over the winter of 1989–90 at W1 with a pair of Aanderaa RCM5s. In 1989, the data recovery was about 65%; in 1990 it was about 90%. In 1989, four of the near-surface instruments were lost to fishing activity though no moorings were lost.

Drifters were tracked in Conception Bay in 1987, 1988, 1989 and 1991. Several different types of drifters were released in a variety of configurations at different times and places within the study area (Table 1). ARGOS drifters that track the surface 1 m of the water column were deployed in 1987. In 1988 and 1989, drifters equipped with radar reflectors were tracked using ship radar. These drifters were usually drogued in the top 10–20 m of the water column. Two types of tracking were used for the radar-reflecting drifters. Type 1 tracking consisted of obtaining drifter positions from photographs of the ship's radar referenced to the ship's heading and position, and was used for tracking a small cluster of many drifters. Type 2

tracking consisted of driving the ship alongside each drifter and using the ship's LORAN-C to position the drifter. This mode of tracking was used when drifters were dispersed over wider areas throughout the bay. In 1989 and 1991, drifters equipped with LORAN-C navigation were used. These drifters tracked the surface mixed layer, with drogues spanning the depth range 5–15 m.

The only suitable wind data for the bay were measured at St John's Airport, about 15 km to the east. Correlations between a short record of wind data collected near the head of the bay revealed *r*-squared correlations of 0.8 to 0.9. The St John's wind data have also been tested in a reduced-gravity model of the wind-forced response of the bay reproducing much of the observed response in the bay at periods of 2–10 days (deYoung et al., 1993b).

### 3 Hydrography and seasonal variations

Contours of temperature, salinity and density along the axis of Conception Bay are shown in Fig. 3, where the plots are for April 1989, when there was no ice present, but are representative of the springtime structure. The 0°C isotherm is near 25-m depth over most of the bay, with surface temperatures from 1 to 2°C. During this spring period, there is no appreciable along-bay surface temperature gradient. Lower surface salinity is found near the head of the bay, with a deeper and sharper pycnocline present there as well. Near the head  $\Delta\sigma_t$  from 25 to 50 m is  $\sim 0.35$  whereas near the mouth  $\Delta\sigma_t$  over the same depth range is only  $\sim 0.15$ . The head of the bay is sheltered from the winds in the spring resulting in reduced vertical mixing near the head as compared with the outer bay and the adjacent shelf.

Below 50 m there is little thermal stratification, a result of winter cooling, which causes vertical convection down to depths of 100–150 m. Conception Bay is a cold water system. In April 1989, a density intrusion was observed on the slope 35–45 km from the head (Fig. 3). On April 17, water on this slope, at 200- to 225-m depth, had  $\sigma_t = 26.95$  whereas at the bottom of station CC3 (290-m depth)  $\sigma_t$  was 26.75. Eight days later on April 25,  $\sigma_t$  on the slope was 26.77 whereas at the bottom of CC3,  $\sigma_t$  had increased to 26.95, indicating that bottom water renewal had taken place. With the limited data in hand, it is not possible to determine the characteristics of this system that control the bottom water exchange (Gade and Edwards, 1980).

Figure 4 shows the same transect along the axis of the bay in November 1989. Comparison of Figs 3 and 4 shows that the thermocline in the fall is much deeper and thicker than in spring. By November the surface layer that develops over the summer has started to deepen as a result of strong fall winds. The 0°C isotherm is also much deeper, between 125- and 150-m depth compared with 25- to 50-m depth in April (Fig. 3). Bottom water temperatures in November are, however, lower than in April, in spite of the summer heating and increased surface temperatures. In addition, the bottom density is higher by  $0.05 \text{ kg m}^{-3}$ , the result of an increase in salinity associated with inflow of denser water.

Surface water temperature ranges from  $-1.6^\circ\text{C}$  in March to  $13\text{--}17^\circ\text{C}$  in late

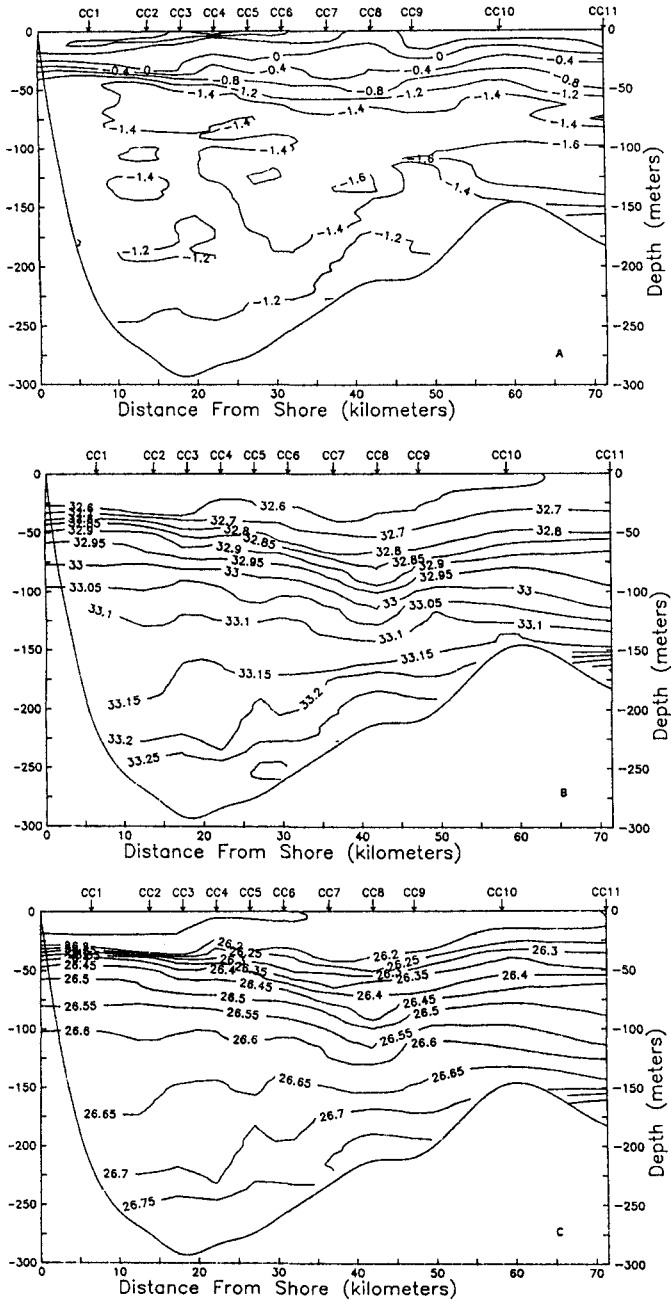


Fig. 3 (a) Temperature, (b) salinity and (c)  $\sigma_t$  along the axis of the bay on 25 April 1989. The station locations are shown in Fig. 2.

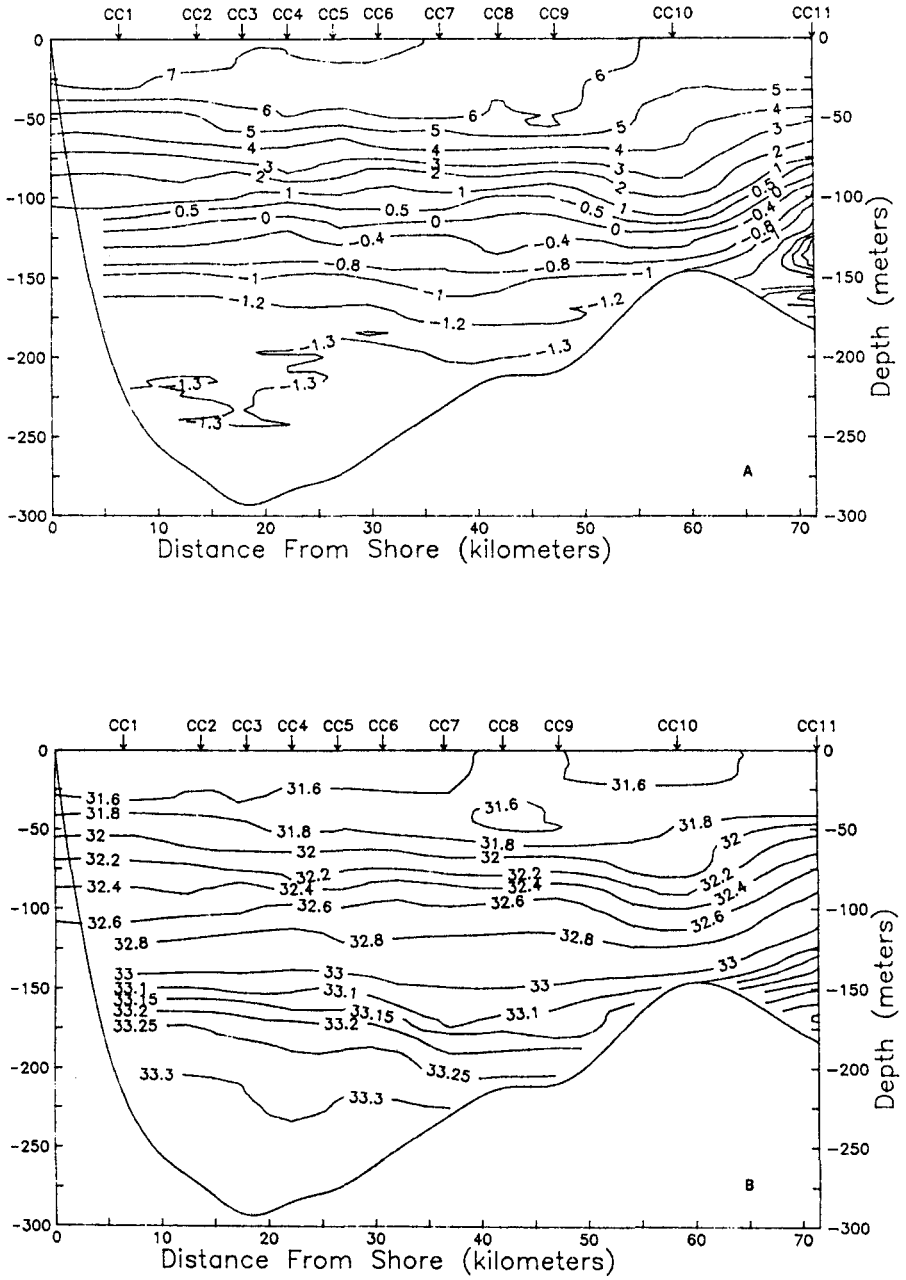


Fig. 4 (a) Temperature, (b) salinity along the axis of the bay on 2 November 1989. The station locations are shown in Fig. 2.

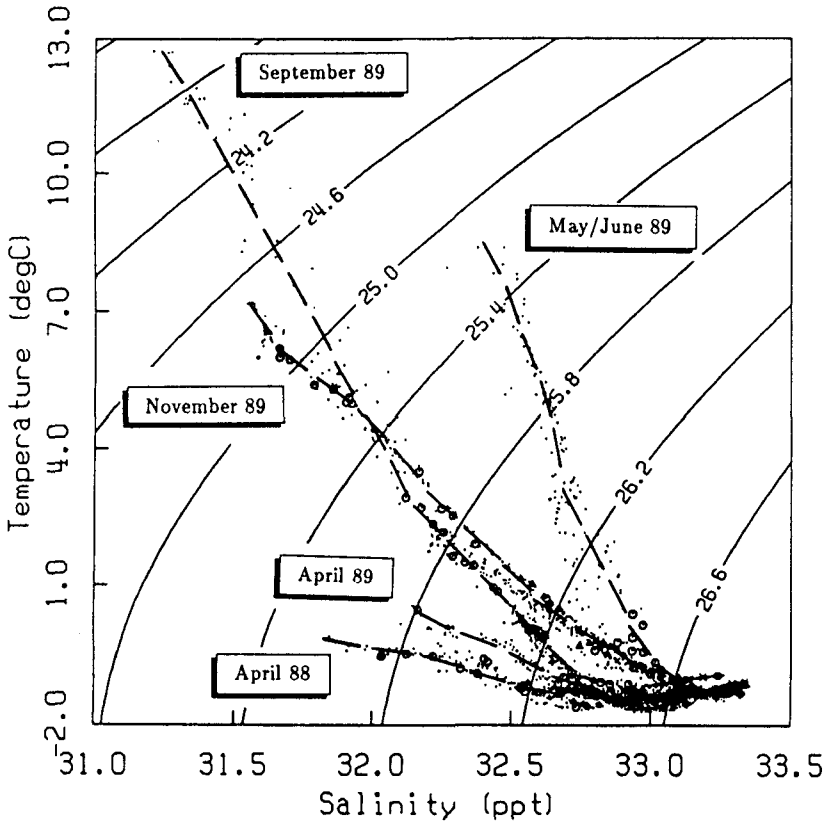


Fig. 5 Temperature versus salinity from CTD profiles at CCI-CC10 along the axis of the bay (Fig. 2a). Points are extracted from the profiles at 5-m intervals for April 1988, April 1989, May/June 1989, September 1989 and November 1989.

August/September. A  $T$ - $S$  plot shows the observed range of temperature and salinity during the period 1988 to 1989 (Fig. 5). From April to May in 1989 there is little change in the surface salinity but an increase of temperature by almost  $9^{\circ}\text{C}$ . The drop in surface salinity from 32.5 to just over 31.0 takes place from May/June 1989 to September 1989. Interannual differences in surface salinity are apparent from April 1988 to April 1989 (Fig. 5).

The surface temperature follows the annual cycle described at Station 27 (Petrie et al., 1991), located just outside St John's harbour about 15 km south of the mouth of the bay (Fig. 1). At Station 27, surface water temperature ranges from  $-1.6^{\circ}\text{C}$  in March to  $16$ – $20^{\circ}\text{C}$  in late August/September. As one might expect, the temperatures in the bay follow closely those observed outside the bay at Station 27. From 1986 to 1991 bottom water ranged from  $-0.8$  to  $-1.4^{\circ}\text{C}$  with no evidence of any seasonal signal. It is expected that the seasonal signal at depth would be

small, as it is at Station 27 (Petrie et al., 1991). The sill, which restricts access to the deep water, will also tend to limit the strength of the seasonal signal.

The temperature maximum in the surface water occurs just before the salinity minimum in September. The observed lag is the same as that observed on the shelf by Petrie et al. (1991), who showed that one must consider the advective transport of fresh water to account for the timing of the salinity minimum in the surface water, something that is also true for temperature (Mathieu and deYoung, 1994). Myers et al. (1990) showed that there is a lag of 3–4 months between sea-ice extent over the Labrador shelf and the observed salinity minimum on the Newfoundland shelf. Thus ice-melt and advection are important influences on the surface salinity and temperatures in Conception Bay, as they are on the shelf.

### 4 Eulerian circulation

The Eulerian current-meter data (Fig. 2b) were collected from spring 1989 to late summer 1990. Two different experiments were conducted. In 1989 moorings were placed inside the bay (M1, M2, M7, M8) and across the mouth (M3–M6) in an attempt to define the mean circulation and the transport across the mouth. Unfortunately, surface current-meter data were recovered from just two of the moorings, M2 and M3, thus limiting the utility of these data for the intended purpose. In the second year, 1990, the moorings were located around the head of the bay (H1–H6) to provide information about the coastal wind-forced response. These data are discussed in more detail in a paper applying a reduced-gravity model to the bay (deYoung et al., 1993b). Over the winter of 1989/90 one current meter was deployed at W1.

The spectra of the currents are red with marginally significant peaks at the dominant tidal frequencies ( $M_2$  and  $K_1$ ) and also at the near-inertial period (roughly 16.2 h). Figure 6 shows the spring–fall time series of current from station M2 (see Fig. 2b) together with wind stress calculated using measurements at St John's airport. These data have been low-pass filtered to remove energy at periods shorter than 40 h. Rotary cross-spectral analysis shows that coherence squared  $\leq 0.4$  between the wind and each of the current time series and between the two current records. There is, however, significant coherence between the currents at the tidal and near-inertial frequencies. The ratio of the variance between the surface and bottom currents, with the tides removed, is approximately 4 for the six 1990 moorings (see Table 2 for data on the means and standard deviations of the surface data). As expected, the bottom currents are much weaker than the surface currents. Throughout the spring–fall period there does not appear to be any persistent mean flow, into or out of the bay, in either the surface or the bottom data. The results from this one location in the bay are representative of the flow field in other locations in the bay. At low frequencies and near the shore, the flow is strongly aligned with the topography except during the summer.

Autocorrelation analysis (Fig. 7) reveals that the  $e$ -folding decorrelation time-scale for the Eulerian current field varies from 2 to 8 d. The analysis shown in Fig. 7

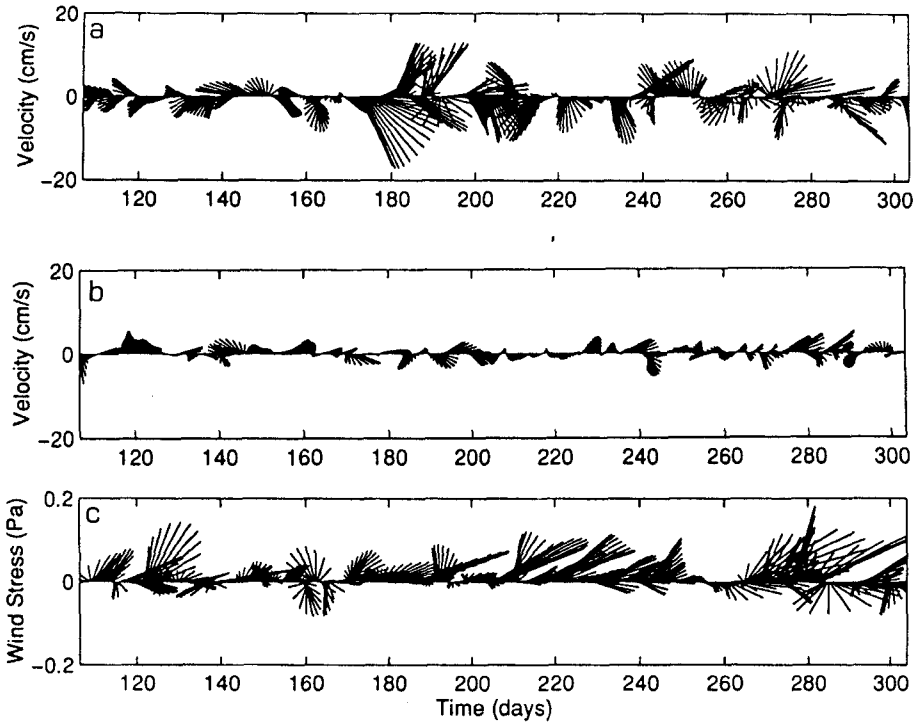


Fig. 6 Stick plots of current at (a) 20 m and (b) 100 m at station M2 in 1989 together with the wind stress as determined from wind measured at St John's airport. Day numbering begins on 1 January 1989. These data have all been low-pass filtered to remove energy at periods below 1.5 d and then subsampled to 6-h intervals. North is at the top. Wind stress is plotted using the oceanographic convention; direction is the direction towards which the wind is blowing.

TABLE 2. Mean velocities with standard deviations for surface currents in Conception Bay as measured at stations H1–H6 (Fig. 2b). The nominal depth of the instruments was 25 m. Energy at periods below 32 h was removed before these statistics were calculated. One standard deviation about the respective means is shown by  $\sigma_u$  and  $\sigma_v$ . Units:  $\text{cm s}^{-1}$ .

Location	$\bar{u}$	$\sigma_u$	$\bar{v}$	$\sigma_v$
H1	-0.0	8.2	0.9	11.0
H2	-1.4	5.2	-1.0	8.3
H3	-0.7	2.6	1.8	6.8
H4	-0.9	4.5	-1.6	3.2
H5	-0.4	4.9	-1.7	4.8
H6	0.1	5.3	0.0	4.4

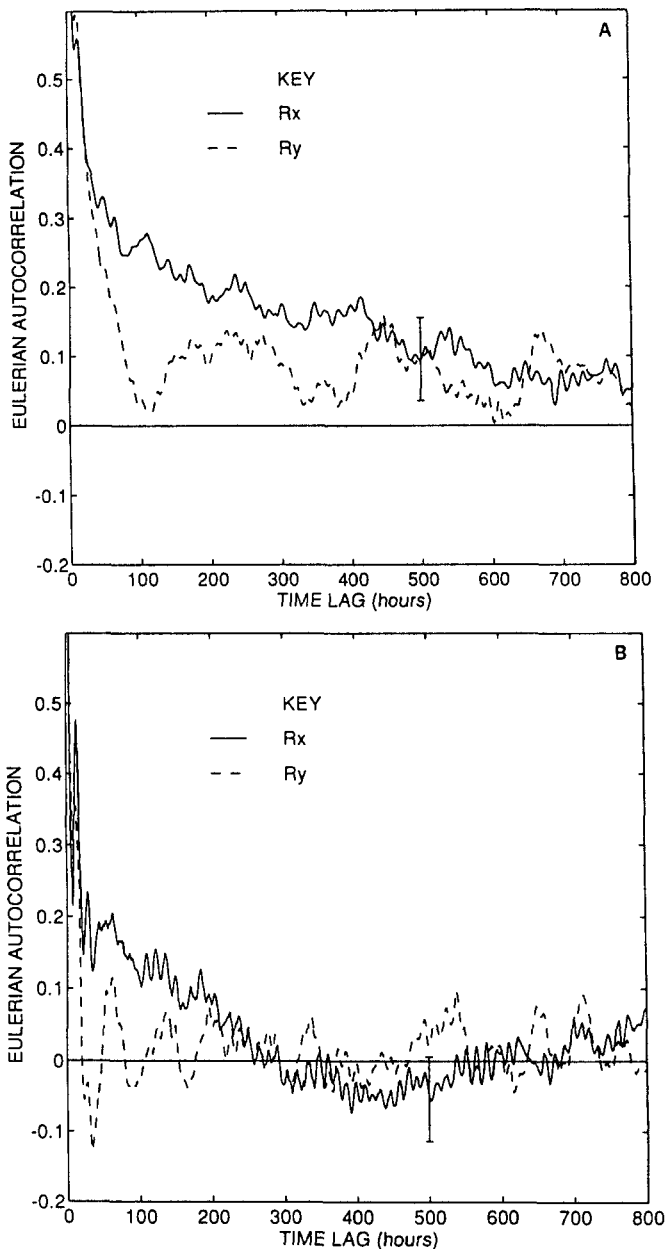


Fig. 7 Eulerian autocorrelation analysis of current-meter data from (a) 20 m and (b) roughly 100 m at stations M1 and W1. The summer record for M1 has been combined with the winter record from W1 to give a time series of roughly 383 d. The error bar in the plot is calculated assuming there are roughly 200 degrees freedom in the record.  $R_x$  is cross-bay and  $R_y$  is along-bay.

was applied to a record obtained by concatenating the summer record from M1 with the winter record from W1 (Fig. 2b) to give 383 d of surface and deeper currents (nominal depths 20 and 100 m). The results from this analysis are broadly consistent with analysis done on other, shorter current records. The cross-bay component ( $R_x$ ) exhibits longer decorrelation time-scales than the along-bay component ( $R_y$ ), and also shows much more tidal influence. The tidal oscillations are more prominent in the deeper (100 m) record, since they make up more of the total variance. The bottom record shows some evidence for an internal response at 3–5 d period that may be associated with an internal seiche. This periodicity is also apparent in the time series plots (Figs 7b and 8b). The period of the internal seiche is roughly  $L/c = 2 \times (70 \times 10^3 / 0.5) = 3.2$  d where the length  $L = 70$  km, and the internal wave speed  $c = 0.5$  m s<sup>-1</sup> is calculated from the vertical density data (deYoung et al., 1993b).

Figure 8 shows the fall–winter time series of wind and currents at a location somewhat closer to the head of the bay (W1 in Fig. 2a). Again there is weak coherence between the different time series, coherence squared  $\leq 0.4$ . In contrast to the spring–fall data, there does appear to be a persistent mean flow into the bay (southwestwards) in the bottom water during fall–winter particularly from the start of 1990 (beyond day 340). During most of this period, the currents alternate from northeastwards (out of the bay) to southwestwards (into the bay). Note that north is at the top in these plots. This inflow at depth (Fig. 8b) is associated with a flow out of the bay in the surface water that is associated with strong wind events beyond day 340; however, strong inflow is observed with winds blowing towards the northeast (around day 390) and the southeast (around day 370). There is not any clear relationship between the direction of the wind and the current response. This inflow of water at depth, and outflow in the surface water, indicates that deepwater exchange is not confined to the spring period.

Analysis of the current-meter data shows that for almost all records, the mean current is smaller than just one standard deviation, with the tides removed. Although the variance in the surface current is greater than that at depth, by a factor of 4, the means have approximately the same amplitude of 0–2 cm s<sup>-1</sup> (see Tables 2 and 3). Plots of the mean currents do suggest that there may be a significant background circulation. A plot of the mean currents from the 1990 near-surface data (Fig. 9a) shows an anti-cyclonic circulation at the head of the bay. The bottom water circulation at the mouth (Fig. 9b), as determined from the 1989 data, shows a cyclonic pattern that is consistent with the surface drifter data (see Section 5). The outflow in this northeast corner of the bay is consistent with earlier observations reported by Aggett et al. (1986). These mean current patterns need to be interpreted with some caution because of the strength of the variability, but the data do form a consistent pattern.

Even if we cannot be sure of the mean current pattern, we can infer something about the nature of the circulation by looking at the orientation of the currents in different parts of the bay. Figure 10 combines all the surface data for the bay

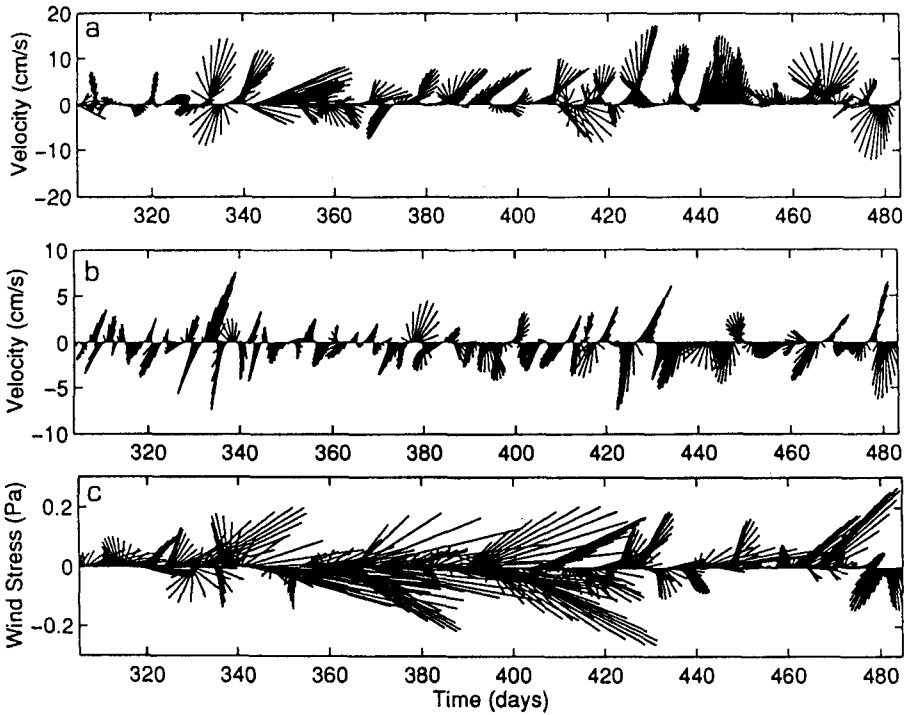


Fig. 8 Stick plots of current at (a) 25 m and (b) 200 m at station W1 in 1989/90 together with the wind stress as determined from wind measured at St John's airport. Day numbering begins on 1 January 1989. These data have all been low-pass filtered to remove energy at periods below 1.5 d and then subsampled to 6-h intervals. North is at the top. Wind stress is plotted using the oceanographic convention; direction is the direction towards which the wind is blowing.

TABLE 3. Mean velocities with standard deviations for bottom currents in Conception Bay as measured at stations M1–M8 (Fig. 2b). Bottom measurements were all made at depths greater than 100 m. Energy at periods below 32 h was removed before these statistics were calculated. One standard deviation about the respective means is shown by  $\sigma_u$  and  $\sigma_v$ . Units:  $\text{cm s}^{-1}$ .

Location	$\bar{u}$	$\sigma_u$	$\bar{v}$	$\sigma_v$
M1	-0.1	2.2	-0.6	3.9
M2	0.4	3.6	0.1	3.2
M3	0.5	4.8	-0.2	7.1
M4	-1.5	4.1	-1.9	5.2
M5	-2.3	5.3	0.3	3.9
M6	-0.1	4.5	1.4	4.4
M7	0.1	3.0	0.5	2.8
M8	0.9	3.8	0.9	3.9

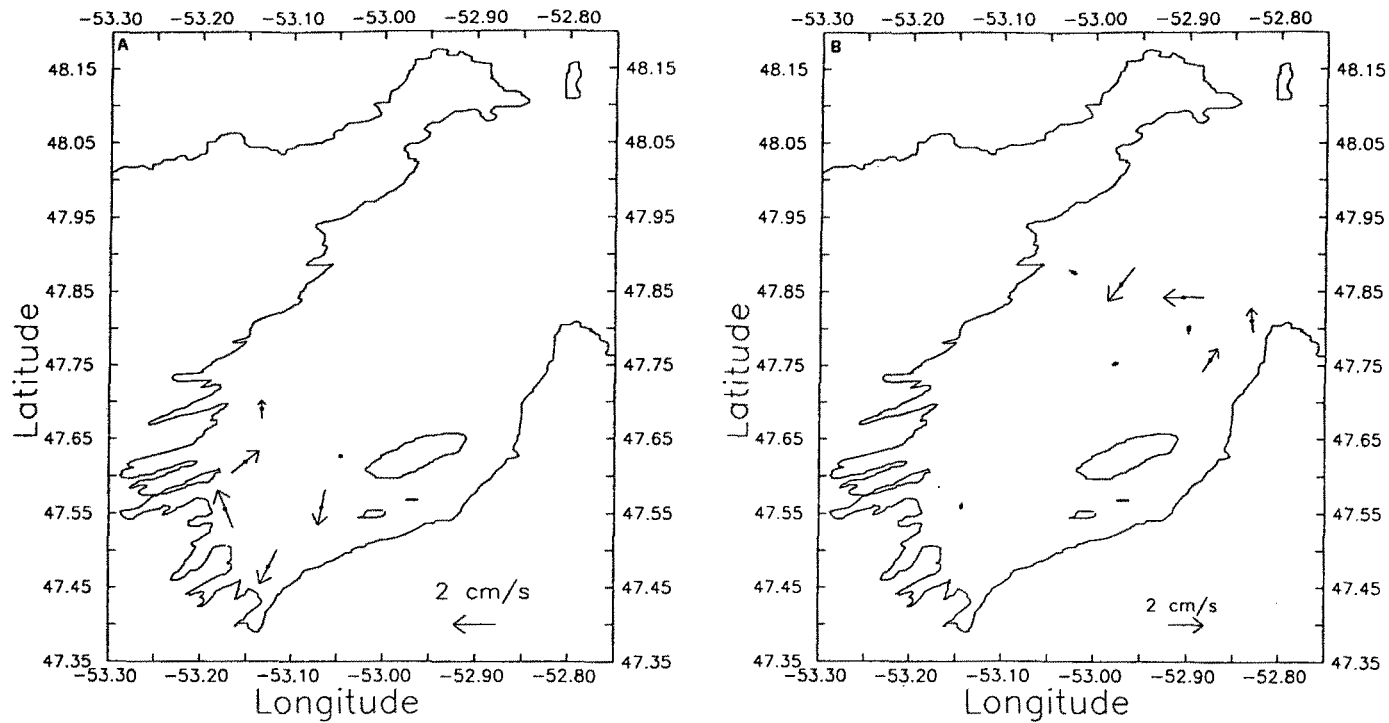


Fig. 9 Mean currents in the bay (a) at the surface (25-m depth) in 1990 from the full time series (days 130–190) and (b) at the bottom in 1989 as determined from the full time series (days 110–280).

## Circulation and Hydrography of Conception Bay, Newfoundland / 151

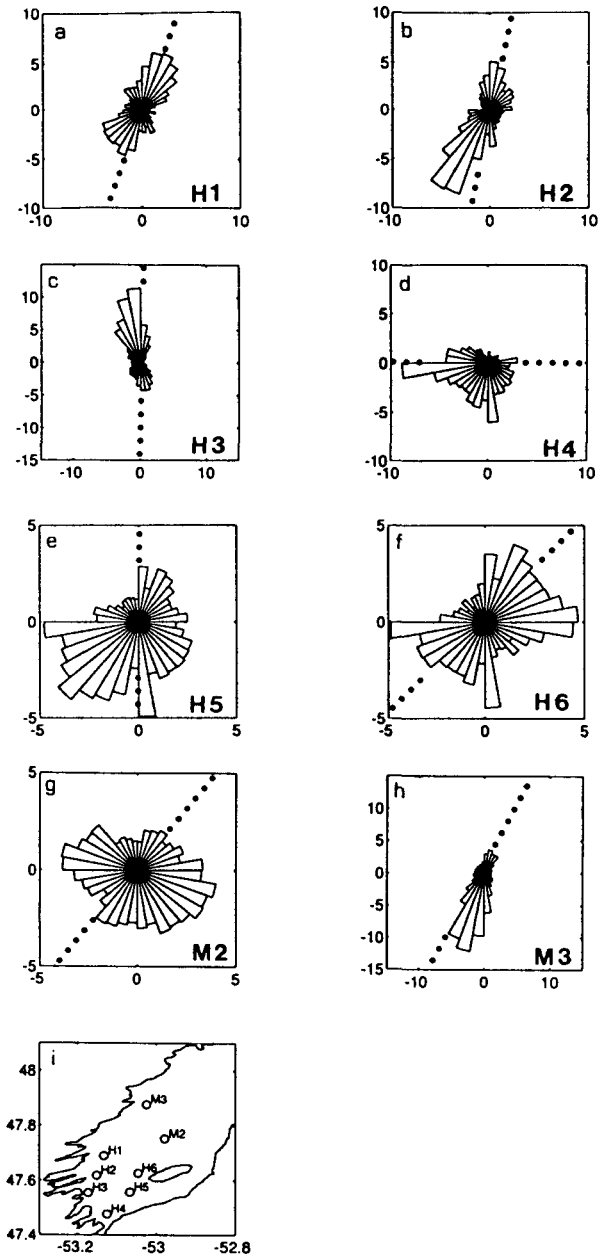


Fig. 10 Current rose plots indicating the distribution of current directions for the combined 1989 and 1990 data. Only the surface currents are shown for stations (a) H1, (b) H2, (c) H3, (d) H4, (e) H5, (f) H6, (g) M2 and (h) M3. The solid dots show the alignment of the bottom topography at the mooring location.

from 1989 and 1990. Current rose diagrams show the distribution of direction observations in the data. Observations near the shoreline (H1–H6) show that the flow is guided by the coastal and bottom topography, with the line of the topography indicated in the plots. The one exception to this case is at H4 near the head of the bay, where the mean flow appears to be directed shorewards, as part of what may be the anti-cyclonic circulation referred to above. At the mouth of the bay, near M3, the flow is primarily directed into the bay. In the centre of the bay, near M2, there is no preferred orientation to the flow. These rose diagrams together with the mean circulation plot, present a picture of the circulation in which the flow near the shoreline oscillates parallel to the coastline but the flow in the middle of the bay is variable with no preferred direction and no well defined persistent circulation pattern.

### 5 Lagrangian circulation

A composite map of all drifter velocities on a 4 km × 4 km grid is shown in Fig. 11a. Experiments consisting of many drifters in a small cluster were subsampled to reduce the number of drifters, so as not to bias estimates of the mean flow field. Also, different experiments obtained positions with different frequencies. Hence we subsampled the data so that drifter velocities were measured over  $5 \pm 1$  h intervals. Figure 11b shows the local mean flow field obtained by averaging velocity vectors in each grid of Fig. 11a. For most of the bay the mean currents are weak. This is particularly the case near the head of the bay, in the central bay, and along its western side. In these areas the mean current vectors are often oriented in opposition to neighbouring vectors, which further suggests that the true mean currents are smaller than those inferred from our limited data. Current meters typically give mean velocities less than  $2 \text{ cm s}^{-1}$  at 25-m depth in these areas, as discussed earlier.

In periods of dominantly southwesterly winds we often observed that drifters move out of the bay in the shallow area near Bell Island, Little Bell Island and Kellys Island. There is often an eastwards flow across the outer bay north of Bell Island and out of the bay on its eastern side from the northern tip of Bell Island to Cape St Francis. Drifters leaving the bay in this area usually track within 2 km of the eastern coast at speeds of 10 to  $20 \text{ cm s}^{-1}$ . This flow is consistent with knowledge of local fishermen, for whom it has been a favoured site for trap fishing. Figure 11 shows a mean southwards flow in the Avalon Channel that is consistent with the inshore branch of the Labrador Current (Petrie and Anderson, 1983).

Through most of the bay the currents have a small mean value compared with their variability. It is, therefore, important to determine the structure of the variable flow and its scales of variability in order to understand and quantify transport within the bay. Many of the drifter tracks used to compile Fig. 11 are inadequate for studying anything but the simplest properties of the flow field because of poor position-fixing accuracy or too short a tracking period. The following work presents an analysis of one set of drifter observations well suited for examining the

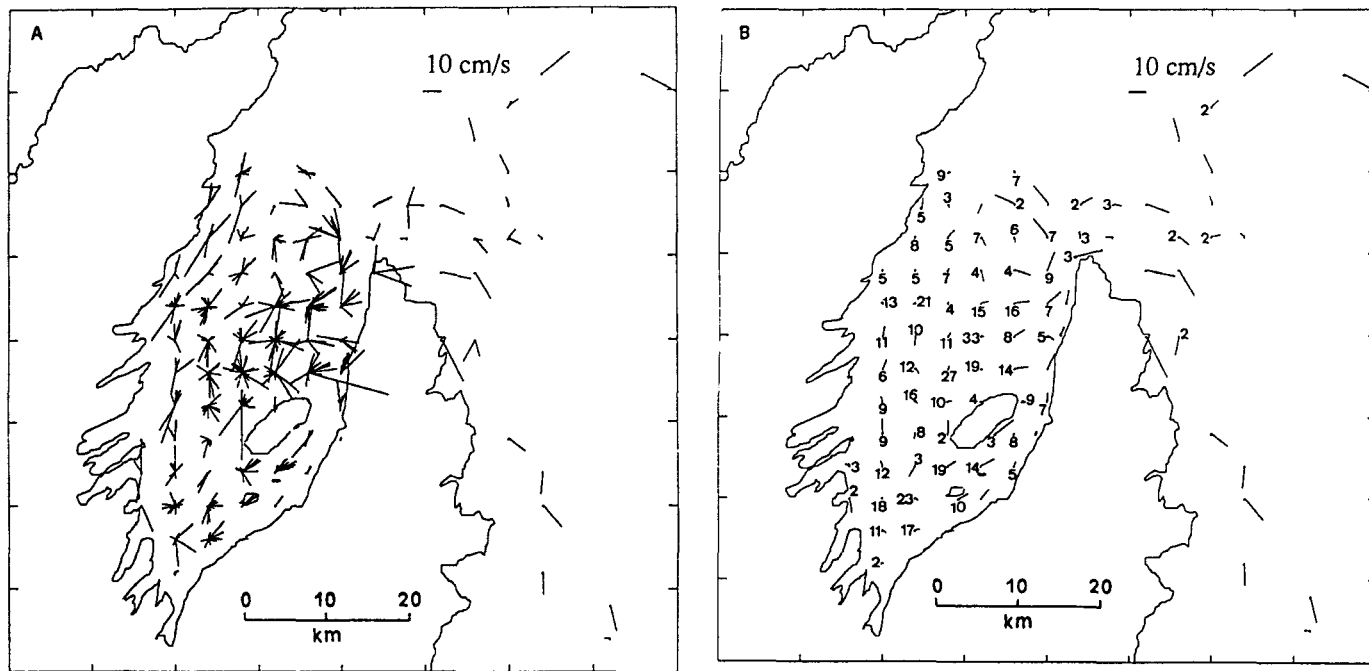


Fig. 11 (a) Current vectors from all drifter data. (b) Mean Lagrangian Currents. A  $10 \text{ cm s}^{-1}$  speed scale is shown near the top of each plot. Complete information regarding start and end times, number of drifters and locations for the data used in the generation of this figure is given in Table 1. The vertical axis of each plot is aligned with north. Tick marks on the plot axes indicate 10-km intervals. The number at the base of each of the vectors in (b) indicates the number of velocity measurements used to generate the average. Vectors in (b) without numbers were based on 1 velocity observation.

nature of variable currents in the bay and the role they play in transporting material within the bay.

The drifter trajectories from the July 1991 deployment of 6 LORAN-C drifters are shown in Fig. 12. All 6 drifters were tracked over the same 10-d interval. Drifters deployed close together frequently have markedly different paths and mean displacements. In Fig. 12a a drifter on the western side of the bay moves first into the bay, then out and finally into the bay. It would be difficult to determine some mean flow pattern from these drifter tracks but we do see evidence of cyclonic eddy structures, especially on the eastern side near the mouth of the bay. The one drifter that migrates cyclonically towards the head of the bay suggests a circulation pattern associated with a coastal jet but, on other occasions, drifters in the same vicinity tracked in the opposite direction and current-meter measurements sometimes suggest a mean anticyclonic circulation at the head of the bay.

The mean Lagrangian velocity was obtained from the average over all 6 drifter trajectories plotted in Fig. 12 and then averaging over the duration of the experiment. The mean Lagrangian along- and cross-bay components are  $(0.3 \text{ cm s}^{-1}, 0.0 \text{ cm s}^{-1})$  where, for the present purposes, we use an orthogonal right-handed coordinate system with the  $y$ -axis aligned along the axis of the bay ( $\sim 25^\circ$  relative to true North). The root-mean-square values for components of velocity relative to this mean are  $(5.8 \text{ cm s}^{-1}, 6.8 \text{ cm s}^{-1})$ , indicating very little anisotropy.

Lagrangian velocity autocorrelations give fundamental information about eddy dispersion and transport (Taylor, 1921). Figure 13 shows the Lagrangian autocorrelation functions  $R_{Lij}(\tau)$  and  $h_L(\tau)$  calculated from drifter velocity  $u_i (i = 1, 2)$  relative to the above Lagrangian mean for lags up to 100 h.

$$R_{Lij}(\tau) = \langle u_i(t)u_j(t + \tau) \rangle / V_L^2$$

$$h_L(\tau) = [R_{L12}(\tau) - R_{L21}(\tau)]/2$$

$$V_L^2 = \langle u_i^2 \rangle / 2.$$

The zero-crossings are at 18 and 23 h for the  $x$  (along-bay) and  $y$  (cross-bay) components of motion; however, these are followed by statistically significant oscillations at larger lags.

The simplest and most widely used way to characterize transport due to variable flow is in terms of the Lagrangian integral time-scale and the eddy diffusivity. Integrating over lags up to 100 h gives integral time-scales of 5.3 h for the cross-bay motion and 6.1 h for motion along the axis of the bay. This corresponds to diffusivities of  $63$  and  $102 \text{ m}^2 \text{ s}^{-1}$  across and along the axis of the bay, respectively. Over a 10-d period the above mean currents cause displacements of  $\sim 2$  km, whereas the above eddy-diffusivities cause dispersion over distances of  $\sim 10$  km from the initial positions. Figure 12 shows that, over 10 d, the drifters typically dispersed over distances of  $\sim 25$  km from their release position. The separation of the flow

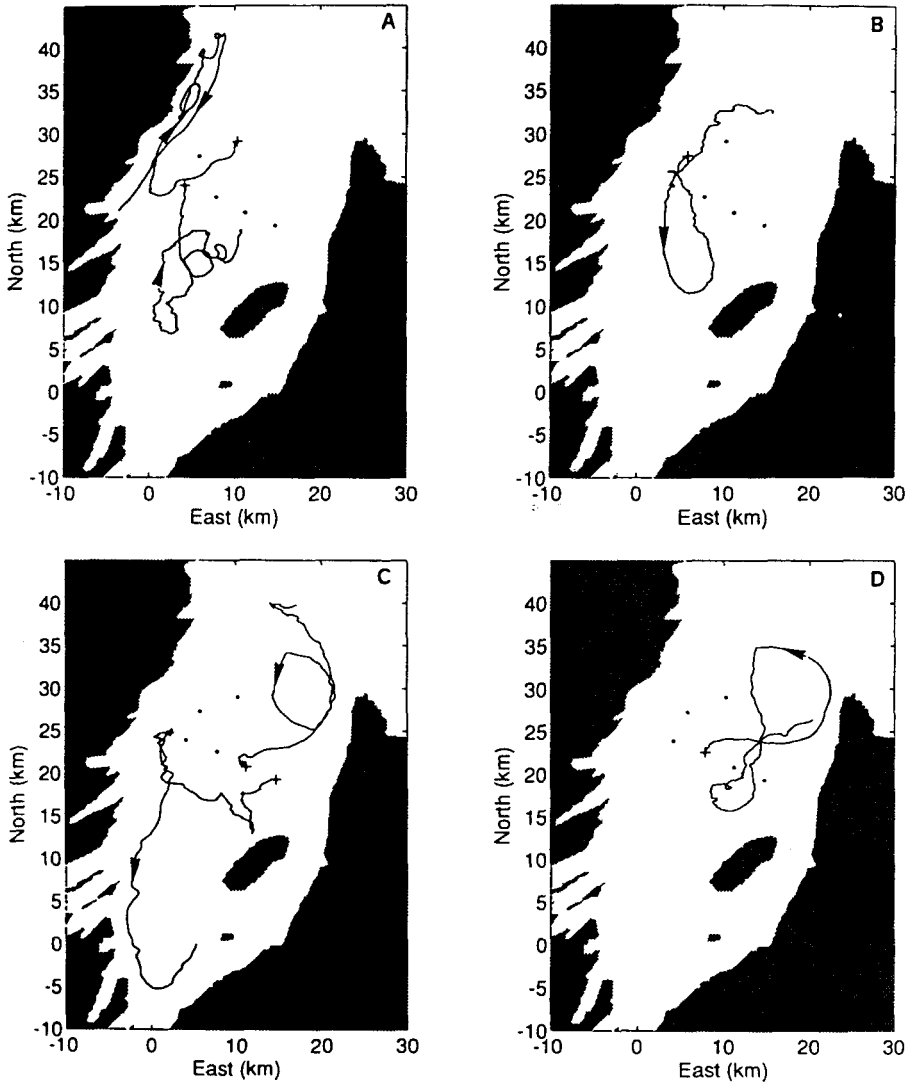


Fig. 12 Trajectories of 6 LORAN-C drifters from 3 to 13 July 1991. The origin of each trajectory is marked with a cross. Dots show release positions of drifters on other plots and arrow heads indicate the direction of motion.

field into a mean advection and fluctuating motion parameterized as an eddy diffusion is a simplistic way of approximating the Lagrangian transport and its variability, because the flow field has structure at all space and time-scales.

Trajectories in Fig. 12 suggest that although there may not be any mean Lagrangian flow, there is a tendency for the cyclonic drifter tracks. The mean angular

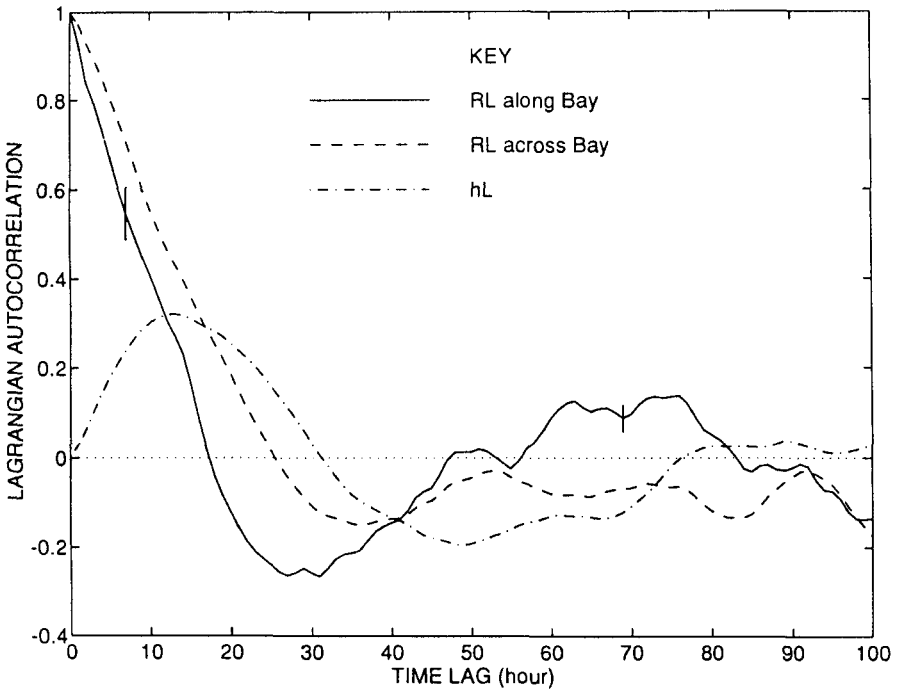


Fig. 13 Lagrangian autocorrelation function of drifter velocities obtained from the 6 trajectories plotted in Fig. 12. The solid and dashed lines show  $R_L$  for  $x$  and  $y$  components of motion respectively. The dot-dashed lines shows  $h_L$ . The vertical bar indicates plus and minus one standard deviation.

momentum  $J$  of the flow field is related to  $h_L(\tau)$  by (Middleton and Garrett, 1986)

$$\frac{\partial J}{\partial t} = V_L^2 h_L(\tau).$$

The plot of  $h_L$  (Fig. 13) shows that the Lagrangian flow is increasingly cyclonic as lags increase to 30 h and becomes less polarized for larger lags.

The above Lagrangian analysis is most useful for determining transport but Eulerian properties are often more convenient for visualizing the flow structure and understanding the flow dynamics. Single-particle Eulerian statistics will, therefore, be computed from the July 1991 data (Fig. 12). Correlating the velocity at position  $\mathbf{x}$  and time  $t$  with a velocity at position  $\mathbf{x} + \mathbf{r}$  and time  $t + \tau$  gives information about both the spatial and temporal Eulerian structure of a variable flow. Velocity is split into a longitudinal component  $u_L$  along the direction of  $\mathbf{r}$  and a transverse component  $u_T$  perpendicular to  $\mathbf{r}$  in a right-handed coordinate system. Note,  $u_L$  and  $u_T$  are components relative to the direction of the separation vector  $\mathbf{r}$ . There are insufficient observations to calculate velocity correlations as functions of the two

## Circulation and Hydrography of Conception Bay, Newfoundland / 157

components of  $\mathbf{r}$  as well as the time lag for  $\tau$ . Consequently we follow Middleton and Garrett (1986) and calculate functions  $f(r, \tau)$  and  $g(r, \tau)$  for the correlations of longitudinal and transverse components of motion as functions of separation scale  $r = |\mathbf{r}|$  and time lag  $\tau$ .

The estimates of  $f$  and  $g$  plotted in Figs 14a and b typically have standard deviations of 0.1. The longitudinal motion is positively correlated for spatial lags of order 10 km, although the correlation becomes weak at separation scales larger than 4 km. This high correlation of longitudinal motion at small spatial lags applies to time lags from 0 to 30 h. The transverse motion is positively correlated for separation scales up to 3–4 km and time lags up to 40 h. The Lagrangian integral time-scales are smaller than the Eulerian time-scales, as might be expected given the small Eulerian eddy length scales.

Figure 14c is a plot of the helicity function  $h(r, \tau)$ , which is obtained from the cross-correlation of lagged longitudinal and transverse components of motion (Middleton and Garrett, 1986). The helicity is positive, indicating cyclonic motion for time-scales of about 1 d and separation scales up to 20 km. These cyclonic eddies are some of the larger-scale coherent flow structures of the Eulerian eddy flow field.

The above analysis reveals typical statistical properties of the eddy field. Let us now examine the occurrence and properties of specific eddies. In the outer bay, drifter trajectories showed cyclonic eddies once in July 1989 and three times in July 1991. Trajectories indicating anticyclonic eddies in the outer bay were observed once in September 1987 and once in July 1991. The cyclonic trajectory of the LORAN-C drifter in July 1989 is our best example of a drifter tracking a cyclonic eddy in the outer bay because of the high quality of the position fixes and because the drifter tracked the eddy for 66 h after which it was ejected into a flow out of the bay.

The vorticity and other kinematic properties of the eddy flow field can be calculated from a drifter track using the method outlined by Kirwan et al. (1984, 1988), Halide (1992), and Kirwan (1992). This method of analysis assumes the flow field can be expanded as a Taylor series in position relative to a flow centre at the centre of the eddy and has been used extensively to study warm core rings (Kirwan et al., 1984, 1988). The flow centre tracks the centre of the “elliptical” drifter track. The eddy centre is moving generally northward with a peak speed of about  $0.04 \text{ m s}^{-1}$ . In contrast the swirl velocity (motion about the flow centre) rotates cyclonically with an amplitude of about  $0.15 \text{ m s}^{-1}$  and a period of 23 h. The eddy has large cyclonic vorticity of  $1.2 \times 10^{-4} \text{ s}^{-1}$  which changes by less than 10% in a 60-h period. Divergence, stretching deformation and shearing deformation are all at least an order of magnitude smaller than the vorticity, indicating quasigeostrophic dynamics.

Mean currents are weak throughout most of the bay. The currents have small spatial coherence scales and fluctuate with time. On this basis  $\sim 150$  drifters would be required to determine the near-surface velocity everywhere in the bay. Thus we see

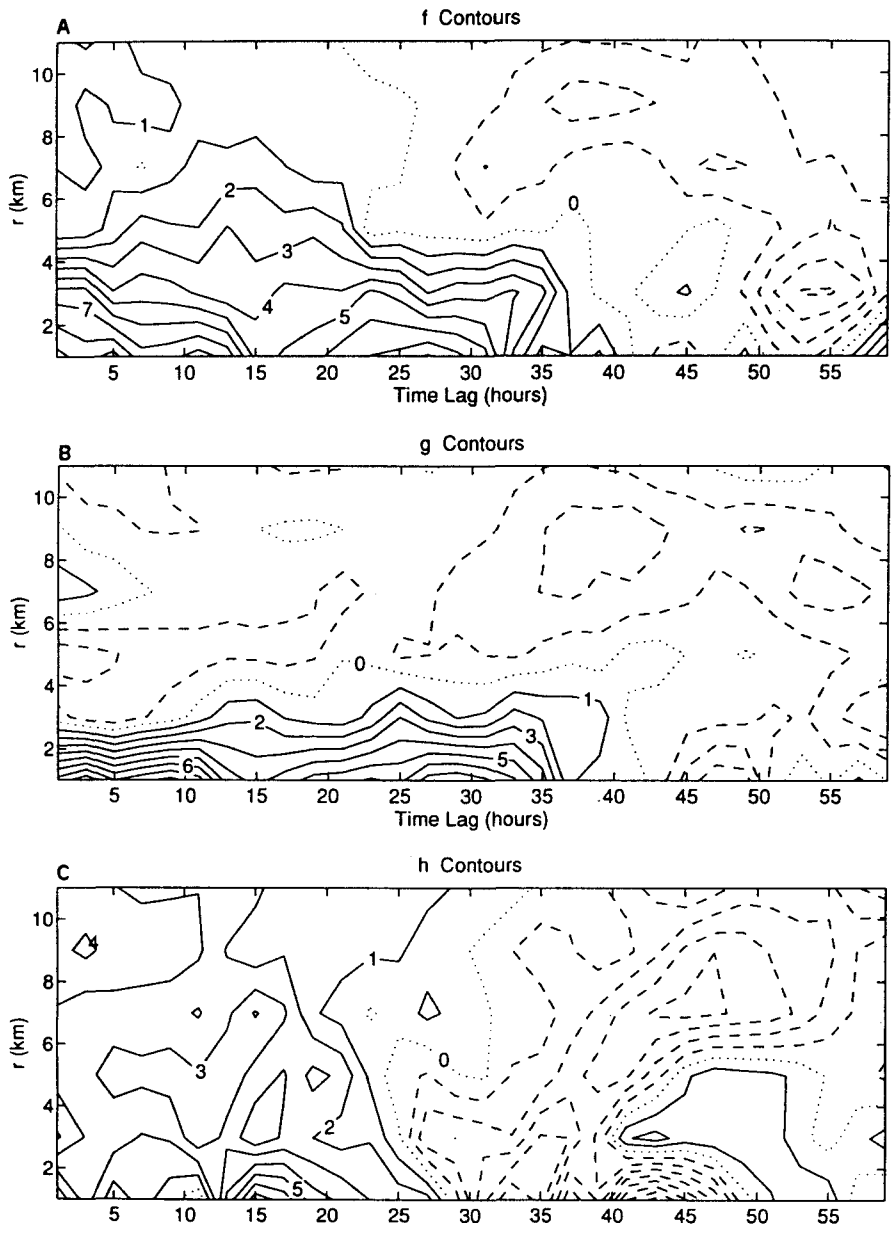


Fig. 14 Eulerian statistics computed from the 6 drifter trajectories in Fig. 12. The plots from top to bottom show contours of the space-time correlation functions  $f$ ,  $g$  and  $h$ , respectively. The contours 0.8, 0.6, ..., 0, ..., -0.4 are numbered at 10 times their value. Shading goes from darker at positive correlations to lighter at negative correlations. The standard deviation of correlations is of order 0.1.

that in Conception Bay the Lagrangian trajectories might be considered stochastic, even if drifters move in response to a deterministic (but spatially and temporally variable) Eulerian flow field. Nevertheless, the Eulerian flow field appears to be relatively strong near the eastern coastline of the outer bay, and consequently the Lagrangian transport might be locally well described as an advective transport.

## **6 Scaling discussion**

The data presented show that there is no strong and persistent mean circulation in Conception Bay. In some parts of the bay, for example, at the surface near the head and near the mouth of the bay on the eastern side, there is a weak mean circulation pattern. The drifter data obtained, and the weak spatial coherence in the Eulerian currents, show that there is much spatial and temporal variability in the bay. What then are the important scales and what terms, advection or horizontal diffusion, are most important?

The time-scale for horizontal eddy diffusion  $K_H = 100 \text{ m}^2 \text{ s}^{-1}$  to transport material over the horizontal dimensions  $L = 70 \text{ km}$  of the bay is  $\sim 280 \text{ d}$ . In contrast a mean advection speed of only  $5 \text{ cm s}^{-1}$  would advect material through the bay in only 16 d. The drifter data collected during 10 d in July 1991 suggest that the mean flow is less important than diffusion, where the mean speed is determined from the full set of drifter data. The scale analysis appears to contradict this result since it suggests that brief events (of several days) with large means (of several centimetres per second) may be important in moving water out of, or into the bay, thereby setting the residence time. The spectrum of horizontal motion is, however, continuous and both high and low frequency motions can have small spatial correlation scales. Consequently there is no theoretical basis for dividing the horizontal transport into a mean advection and horizontal eddy diffusion. We shall, therefore, discuss two different approaches. The first uses a diagnostic calculation of the flow field, from high resolution measurements of the density field, to calculate the temporal and spatially variable flow field explicitly and thereby advect material to determine residence times. The second is a simple calculation that uses the fractal properties of the horizontal Lagrangian motion to estimate residence times for the bay. Both give similar results.

A numerical model that applied a diagnostically calculated, hence fixed, velocity field showed that the residence time depends upon variability in the velocity field and/or diffusion (deYoung et al., 1994). One role of horizontal diffusion is to minimize the influence of any closed circulation features. The velocity field was calculated diagnostically using the density data from the CTD grid shown in Fig. 2a together with the mean wind for the period. The mean residence time for a patch of surface water near the head of the bay was found to be  $\sim 30$  days. Horizontal diffusivities ranging from 1 to  $100 \text{ m}^2 \text{ s}^{-1}$  were used. Residence times decreased with increasing horizontal diffusivity, with a particularly sharp dropoff in the residence time for diffusivities above 1 to  $10 \text{ m}^2 \text{ s}^{-1}$ .

The residence time can also be estimated from the mean surface current. A

mean current speed of  $\sim 2 \text{ cm s}^{-1}$  (see Table 2) gives a residence time of 40 d, comparable with the estimate produced by deYoung et al. (1994). This estimate of mean current speeds is based upon a steady-state mean, averaged over a period of over 100 d. During the same period the standard deviation can be 1–10 times the means speed. In Conception Bay, the mean current depends upon the time-scale over which we choose to average.

A much simpler statistical calculation of the residence time can be made by using a fractional Brownian motion model for the drifter tracks. Fractional Brownian motion models (Sanderson and Booth, 1991) allow for the existence of long time-scales of variability in the Lagrangian motion, such as would be expected from a shear-diffusion model, or the above diagnostic calculation. Recognition of the fractal geometry of particle trajectories enables a simple treatment of dispersion in flows where Lagrangian integral scales cannot be unambiguously determined. In this sense, the fractal view point does for dispersion in self-similar turbulent flows what Taylor (1921) did for dispersion in stationary homogeneous turbulent flows.

The six trajectories in July 1991 give an average divider dimension of  $1.2 \pm 0.1$ . This is smaller than, but similar to (within experimental error), values obtained by Osborne et al. (1989, 1990), Sanderson et al. (1990) and Sanderson and Booth (1991). A fractional Brownian motion will cause a variance in particle position that grows proportional to time raised to a power equal to twice the reciprocal of the fractal dimension (Sanderson and Booth, 1991). Thus we obtain the root-mean-square distance (in km) diffused over as the following function of time (in h)

$$\langle x^2 \rangle^{0.5} = 0.22t^{0.833}$$

where the constant 0.22 is chosen to give root-mean-square velocities of  $6 \text{ cm s}^{-1}$  for velocities obtained from a 1-h sampling interval. This model is therefore based on the above fractal dimension of the drifter tracks and upon the measured root-mean-square value of the velocity components (determined earlier). Sanderson and Booth (1991) provide details on the application of a fractional Brownian motion model to drifter dispersion. The model give a time-scale of 22(42) d for horizontal Lagrangian transport over the 40(70) km length scale of Conception Bay. The fractional description is an incomplete description of the true flow field and does not, for example, contain the clearly discernible cyclonic eddies mentioned earlier. In addition, the fractal model makes no allowance for a mean circulation. In spite of these deficiencies the residence times are similar to those calculated from the diagnostically calculated flow field (30 d).

## 7 Summary

In this paper we present CTD, current-meter and drifter data for Conception Bay, Newfoundland. These data cover the period 1988 to 1991 and provide information about the hydrography and circulation of the bay. Eulerian and Lagrangian current data show that the standard deviation of the surface currents ( $2\text{--}11 \text{ cm s}^{-1}$ ) is

much larger than the mean (0–2 cm s<sup>-1</sup>). Mean currents are weak throughout the bay, although in some locations mean currents do appear to be significant. In most locations the direction of the flow is controlled by the topography. The basin shape in particular plays a significant role in defining the characteristics of the flow field. Tides in the bay are weak, with M<sub>2</sub> and K<sub>1</sub> constituent velocities of 1 to 2 cm s<sup>-1</sup>. Deep current records indicate a possible internal seiche with a period of 3–5 d.

The Lagrangian drifter data reveal an integral time-scale of roughly 6 h, with zero-crossings in the auto-correlation function at from 18 to 23 h. Spatial scales of correlation are short, somewhere between 4 and 8 km depending on the location and type of data analysed. Eulerian data show decorrelation time-scales that are much longer (50–200 h) but do show similarly short spatial scales of correlation.

Horizontal diffusivities were estimated from the drifter data to be from 70 to 100 m<sup>2</sup> s<sup>-1</sup>, well within the range of commonly accepted values. Crude estimates for the residence time were provided, developed from different approaches. Simple scale analysis and some Lagrangian analysis suggest residence times of about 40 d. An advection diffusion model of the bay (deYoung et al. 1994), gives residence times of roughly 30 d, approximately the same.

### Acknowledgements

As with all oceanographic field work, there are many people to thank. First, our fellow COPE scientists who participated in many of the cruises discussed here. Second, the technicians and students who supported this work: J. Foley, J. Craig, K. Forward, K. Munroe, D. Foote, S. Collins and T. Otterson. We would also like to thank the officers and crews of the different vessels on which we worked – *Baffin*, *Dawson*, *Shamook* and *Marinus*. Financial support for this work was provided by an NSERC Strategic Grant, the Cold Ocean Productivity Experiment (COPE). Comments from three anonymous reviewers greatly helped to improve the manuscript.

---

### References

- AGGETT, D.; H.S. GASKILL, D. FINLAYSON, S. MAY, C. CAMPBELL, and J. BOBITT. 1987. A Study of Factors Influencing Availability of Cod in Conception Bay, Newfoundland in 1985, Can. Tech. Rep. Fish. and Aquat. Sci., No. 1562, 123 pp.
- ANDERSON, C.A. 1986. Motions driven by buoyancy forces and atmospheric stresses in the Avalon Channel, Newfoundland, Canada. Ph.D. Thesis, Inst. of Oceanography, McGill University, Montréal, Que., 196 pp.
- COTE, P.W. 1989. Ice limits, Eastern Canadian Seaboard. Ice Centre, Climatology and Application Rep., Environ. Can., Ottawa, Ont., 39 pp.
- CSANADY, G.T. 1982. *Circulation in the Coastal Ocean*. Reidel, Amsterdam, 274 pp.
- DEYOUNG, B.; R.J. GREATBATCH and K.B. FORWARD. 1993a. A diagnostic coastal circulation model with application to Conception Bay, Newfoundland. *J. Phys. Oceanogr.* **23**: 2617–2635.
- ; T. OTTERSON and R.J. GREATBATCH. 1993b. The local and non-local response of Conception Bay to wind forcing. *J. Phys. Oceanogr.* **23**: 2636–2649.
- ; J. ANDERSON, R.J. GREATBATCH and P. FARDY. 1994. Advection diffusion modelling of capelin larvae in Conception Bay, Newfoundland. *Can. J. Fish. Aquat. Sci.* **51**: 1293–1307.

- GADE, H.G. and A. EDWARDS. 1980. Deep water renewal in fjords. In: *Fjord Oceanography*, H.J. Freeland, D.M. Farmer and C.D. Levings (Eds) Plenum Press, New York, pp. 453–489.
- HALIDE, H. 1992. Determining flow singularities from drifter trajectories. M.Sc. Thesis, Dep. of Physics, Memorial University of Newfoundland, 152 pp.
- KIRWAN, A.D., JR. 1988. Notes on the cluster method for interpreting relative motions. *J. Geophys. Res.* **93**: 9337–9339.
- . 1992. Correlation: Observed and simulated properties of loop current rings. *J. Geophys. Res.*, in press.
- ; W.J. MERREL, J.K. LEWIS, R.E. WHITAKER and R.E. LEHECKIS. 1984. A model for analysis of drifter data with an application to a Warm Core Ring in the Gulf of Mexico. *J. Geophys. Res.* **89**: 3425–3438.
- MATHIEU, Y. and B. DEYOUNG. 1994. Application of a mixed-layer model to the inner Newfoundland shelf. *J. Geophys. Res.*, (in press).
- MERTZ, G.; S. NARAYANAN and J. HELBIG, 1993. The freshwater transport of the Labrador Current. *ATMOSPHERE-OCEAN*, **31**: 281–295.
- MIDDLETON, J.F. and C. GARRETT. 1986. A kinematic analysis of polarised eddy fields using drifter data. *J. Geophys. Res.* **91**: 5094–5102.
- MYERS, R.A.; S.A. AKENHEAD and K. DRINKWATER. 1990. The influence of Hudson Bay runoff and ice-melt on the salinity of the inner Newfoundland shelf. *ATMOSPHERE-OCEAN*, **28**: 241–256.
- OSBORNE, A.R.; A.D. KIRWAN JR., A. PROVENZALE and L. BERGAMASCO. 1989. Fractal drifter trajectories in the Kuroshio extension. *Tellus*, **41A**: 416–435.
- PETRIE, B. and C. ANDERSON. 1983. Circulation on the Newfoundland continental shelf. *ATMOSPHERE-OCEAN*, **21**: 207–226.
- ; J.W. LODER; S. AKENHEAD and J. LAZIER. 1991. Temperature and salinity variability on the eastern Newfoundland shelf: The annual harmonic. *ATMOSPHERE-OCEAN*, **29**: 14–36.
- POMEROY, L.R.; W.J. WIEBE, D. DEIBEL, R.J. THOMPSON, G.T. ROWE and J.D. PAKULSKI. 1991. Bacterial responses to temperature and substrate concentration during the Newfoundland spring bloom. *Mar. Ecol. Prog. Ser.* **75**: 143–159.
- SANDERSON, B.G., A. OKUBO and A. GOULDING. 1990. The fractal dimension of the relative Lagrangian motion. *Tellus*, **42A**: 550–556.
- and D.A. BOOTH. 1991. The fractal dimension of drifter trajectories and estimates of horizontal eddy-diffusivity. *Tellus*, **43A**: 334–349.
- TAYLOR, G.I. 1921. Diffusion by continuous motion. *Proc. London Math. Soc. Ser. 2*, **20**: 196.
-